Fermi surface, effective masses, and Dingle temperatures of $ZrTe_5$ as derived from the Shubnikov—de Haas effect

G. N. Kamm, D. J. Gillespie, A. C. Ehrlich, and T. J. Wieting
Naval Research Laboratory, Washington, D.C. 20375-5000

F. Levy
Institut de Physique Appliquée, Ecole Polytechnique Fédérale de Lausanne, CH-1015 Lausanne, Switzerland
(Received 1 March 1985)

The complete Fermi surface of $ZrTe_5$ has been determined to consist of three independent surfaces: one hole-type (the largest surface) and two electron-type surfaces. The surfaces are all of ellipsoidal form, with at least the electron surfaces mutually nested with common centers and principal axes. In addition, along certain high-symmetry directions, they nearly touch. Within experimental error, the volume of the largest surface is equal to the sum of the volumes of the smaller surfaces. Also determined are the anisotropy of the effective masses, the electron scattering times, and a model of the energy bands as they cross the Fermi level. In the direction of highest conductivity, the effective masses of the electrons and holes are found to be nearly equal and small (3—4 % of the free-electron mass), and the relaxation time for the electrons is more than twice that of the holes.

I. INTRODUCTION

The observation of a large anomalous resistivity peak in both $ZrTe_5$ (at ~ 150 K) and $HfTe_5$ (at ~ 70 K) has generated considerable interest in these materials. Most of the ensuing work has been directed toward understanding the origin of the resistivity peak.[1] Generally, such resistivity peaks are associated with systems which undergo second-order phase transitions. For example, $NbSe_3$ has similar resistivity peaks which are the result of periodic lattice distortions associated with the formation of charge-density waves (CDW). The quasi-one-dimensional structure of $ZrTe_5$ and $HfTe_5$ and the fact that the Hall coefficient and the thermoelectric power both show a change in sign at a temperature close to that of the resistivity maximum suggests that a CDW may be forming at these temperatures. In addition Jackson *et al.*[2] have carried out resistivity measurements at microwave frequencies (2.5 and 9.1 GHz) and reported a strong frequency dependence of the resistivity anomalies. However, the search for clear evidence of such waves has yielded negative results as discussed by DiSalvo *et al.*,[3] Okada *et al.*,[4] and Bullett.[5] X-ray data have so far failed to show the superlattice lines that are expected in a CDW system.[6] Resistivity measurements in the presence of high electric fields (up to 20 V/cm for $HfTe_5$ and 50 V/cm for $ZrTe_5$) have also failed to show behavior associated with the existence of CDW,[1] but these results are consistent with the microwave resistivity data. Although the magnetic susceptibility measurements[3] exhibit a minimum at or near the temperature of the resistivity peak (which could indicate the presence of a CDW), the susceptibility minimum is broader than would be expected for a CDW.

The material $ZrTe_5$ is highly anisotropic. Its crystal lattice is orthorhombic and belongs to the space group *Cmcm*. There are four formula units or 24 atoms in the unit (not the primitive) cell, which has the room-temperature dimensions 3.988, 14.50, and 13.73×10^{-8} cm in the *a*, *b*, and *c* directions, respectively.[7] The Zr atoms lie in the centers of trigonal prisms of Te atoms stacked in the *a* direction, which is the direction of maximum electrical conductivity. The trigonal prisms are coupled in the *c* direction via intermediate Te atom pairs, and in this direction the electrical conductivity is substantially lower.[4] Sheets of trigonal prisms in the *a*-*c* planes are coupled loosely by van der Waals forces in the *b* direction along which the conductivity is minimum. The anisotropy is also reflected in the crystal morphology. Crystals grown by vapor deposition are needles in the *a* direction with a minimum dimension in the *b* direction, and they cleave easily perpendicular to the *b* and *c* directions. As will be seen, the Fermi surface is also highly anisotropic.

Earlier observations[8,9] of the Fermi surface showed a single ellipsoidal surface for both $ZrTe_5$ and $HfTe_5$. In this paper we report on what we think is the complete determination of the Fermi surface of $ZrTe_5$ at low temperature. In Sec. II a brief description of relevant experimental details is given. Section III enumerates a number of procedures developed and then employed to extract our small-amplitude low-frequency Shubnikov—de Haas (SdH) oscillations from background magnetization and noise. In Sec. IV we interpret the SdH spectra and provide the detailed fermiology of $ZrTe_5$. The effective masses, current carrier lifetimes, and the procedures used to obtain them are given in Sec. V. Finally, Sec. VI discusses the implications of our fermiology results for the question of the possible existence of CDW's in $ZrTe_5$.

II. EXPERIMENTAL PROCEDURES

The $ZrTe_5$ crystal used in this investigation was selected on the basis of oscillatory SdH signal amplitude. The crystals were grown from elemental powders having a purity of 99.99% for Zr and 99.999% for Te by iodine-

vapor transport in a two-zone furnace in the manner described by Levy and Berger.[10] The specimen crystal was first adhered to a fused-quartz backing with epoxy cement. Small gold areas for current and potential contacts were then applied by sputtering in argon and lead wires were attached to them by conducting epoxy cement. The sample dimensions are approximately 7 mm$\times$0.1 mm$\times$0.2 mm in the a, b, and c directions, respectively. Potential contacts are separated by 4 mm. The room-temperature resistivity is $\sim$700 $\mu\Omega$ cm and the residual resistance ratio [R(300 K)/R(4.2 K)] is $\sim$6.0. Another measure of sample quality is the prominence of the anomalous peak in the resistivity which occurred at 170 K as illustrated in Fig. 1.

The sample was mounted in a rotating sample holder which allowed arbitrary three-axis positioning. A very exact alignment along the principal directions was achieved by using the fact that the magnetoresistance of $ZrTe_5$ is highly anisotropic. The magnetoresistance is maximum for a field in the b direction, minimum when the field is in the a direction, and a saddle point in the c direction, where it is maximum for rotations towards a and minimum for rotations towards b. This technique yielded alignments along the principal axes a, b, and c, accurate to 0.02°, 0.05°, and 0.1°, respectively. The fact that the magnetoresistance versus the angle was symmetric for all rotations through the principal axes indicates that our crystal is neither twinned nor bent.

The experiments were performed in a variable-temperature magnet Dewar capable of temperatures down to 1.3 K and fields up to 9.6 T. All measurements not related to effective-mass determinations were taken at a temperature of 1.3 K. The magnetoresistance measurements were made by using standard dc four-point-probe techniques. The data acquisition was under computer control and during each field sweep about 1000 data points were accumulated at a spacing approximately linear in $1/H$. Data were accumulated at a large number of magnetic field directions in the three principal symmetry planes. Measurements were made at intervals of at most 15° and, when necessary, as close as every 5°.

III. DATA ANALYSIS METHODS

In most magnetic field directions the SdH oscillations are small and lie on a large and rapidly changing background magnetoresistance as seen in Fig. 2. Exceptions are for high fields in and near the b direction, where the oscillations are large and comparable to the magnetoresistance, and for high fields in and near the a direction, where, although the oscillations are small, the longitudinal magnetoresistance is smaller yet. Before an analysis was made of the oscillatory component of the data, the magnetoresistance background was removed by fitting the data with an appropriately weighted low-order polynomial in $1/H$ and then subtracting this fit from the data. An example of this subtraction process is shown in Fig. 3. In this direction, $H||c$, the oscillations are the smallest relative to the magnetoresistance (roughly 400 times smaller).

The data were then interpolated to yield a fixed number of points (usually 1024) equally spaced in $1/H$ for processing by a fast-Fourier-transform (FFT) program. To improve the spectral resolution the signal amplitude was artificially increased with $1/H$ in order to approximately equalize oscillation amplitudes over the record and digital filtering of the FFT was used to decrease the sidelobes. The magnetic field range was typically 0.6 to 9.6 T, but was individually tailored to reduce noise while preserving the significant data.

Several methods were used to distinguish the SdH peaks in the spectrum from noise. (1) Identical experimental runs were made and the spectra compared. (2) The same data record was processed several ways by cutting off the data at the high- or low-field end. (3) The order and weight of the polynomial fit used to subtract away the background magnetoresistance was varied. (4) The compensation for the exponentially decaying oscillations was changed. Each of these procedures typically has a substantial effect on noise peaks and a much lesser effect on the real spectrum peaks. At times it was also advantageous to modify the digital filtering of the FFT to sharpen the main peak even though sidelobe noise would be thereby increased. Often an otherwise broad spectrum line could be resolved into its individual components.

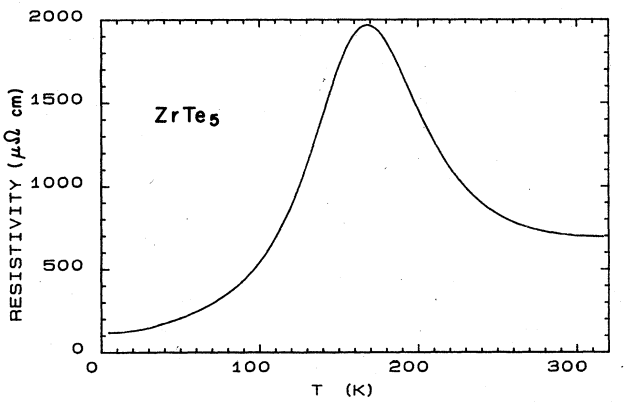

FIG. 1. Resistivity as a function of temperature for $ZrTe_5$ showing the prominent anomaly at 170 K.

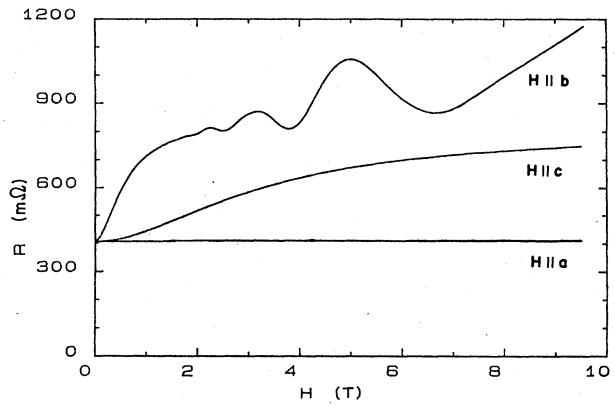

FIG. 2. Magnetoresistance as a function of magnetic field at a temperature of 1.3 K for the principal directions a, b, and c.

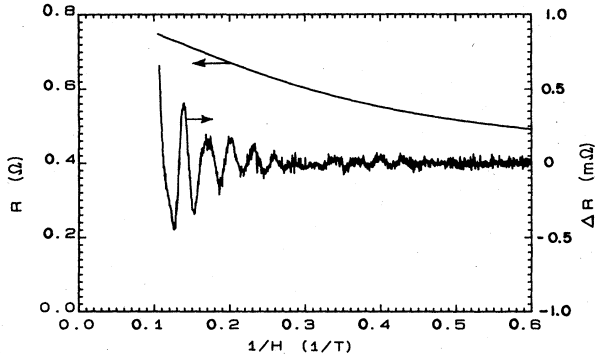

FIG. 3. The upper monotonically decreasing curve shows the magnetoresistance at a temperature of 1.3 K before background subtraction. The lower curve shows the SdH oscillations, now visible, after background subtraction. H is parallel to the c axis.

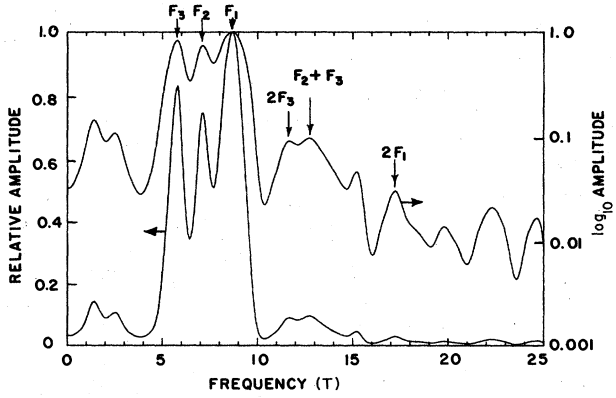

FIG. 5. The fast-Fourier-transform spectrum of the enhanced oscillations of Fig. 4.

IV. SPECTRUM INTERPRETATION AND FERMIOLOGY

A plot of SdH oscillations with background removed for H along b is shown in Fig. 4. It is evident from the appearance of this plot that more than a single frequency is present. A FFT analysis of these data, shown in Fig. 5, and similar data yields SdH frequencies which can all be resolved into three fundamental frequencies, F_1, F_2, and F_3, together with various harmonics and intercombination frequencies, e.g., F_1, $2\times F_1$, F_2, $2\times F_2$, F_3, $2\times F_3$, $(F_2+F_3)/2$, F_2+F_3, etc. Note, however, that combinations of F_1 with F_2 or F_3 were not observed at any field angle. The oscillations associated with F_1 are prominent at high fields and decay rapidly while those associated with F_2 and F_3 persist at lower fields. At some field angles not all of the three fundamental frequencies were observable, perhaps as a result of spin-splitting zeros, but they could be inferred from the presence of their harmonics or combination frequencies. At all angles the relation $F_1>F_2>F_3$ held. The fact that these three frequencies could be followed continuously at all angles of field implies that they originate from just three surfaces, each of which is closed. The relative amplitudes of oscillations associated with F_1, F_2, and F_3 were found to be sample dependent as well as varying with field, temperature, and angle.

The oscillatory component of the magnetoresistance, the SdH effect, is given by

$$\rho_{\rm osc}=\text{const}\times(Fk_BT/\sqrt{H})\{\exp[-\lambda l\mu(T+\chi)/H]\}\times\sin(2\pi lF/H+\phi)\,, \quad (1)$$

where H is the magnetic field intensity, k_B is Boltzmann's constant, F is the frequency in units of T, λ is a constant which is equal to 14.7 T, μ is the effective-mass ratio, T is the temperature in K, χ is the Dingle temperature, and ϕ is a phase angle. The external cross-sectional area of a Fermi surface is proportional to the frequency of the SdH oscillation and is given (in units of m^{-2}) by

$$A=2\pi eF/(hc)\,. \quad (2)$$

The fundamental SdH frequencies obtained from the present study are shown in Fig. 6 as a function of the magnetic field direction. The frequencies range from 6 to

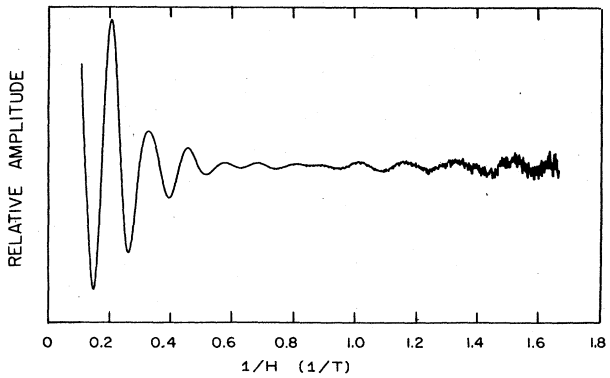

FIG. 4. Magnetoresistance vs $1/H$ at 1.3 K for a field along b. The background has been subtracted and the low-field oscillations enhanced.

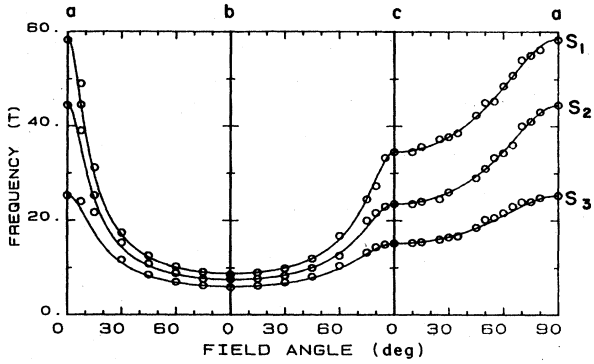

FIG. 6. The fundamental SdH frequencies (proportional to extremal Fermi-surface areas) as a function of field direction in the three principal planes. The solid lines S_1, S_2, and S_3 are the ellipsoidal fit to the circular data points.

nearly 60 T, which is approximately 1000 times lower than the frequency for the belly orbit of copper. The small size of the Fermi surfaces as well as the crystal symmetry suggest the possibility of ellipsoidal-shaped surfaces. The lines drawn through the three sets of data points in Fig. 6 are for three ellipsoids, and they resulted in an excellent fit to the data at all field angles and for each of the three surfaces S_1, S_2, and S_3, designated in order of decreasing size. Cross sections of these ellipsoidal surfaces in the three principal planes are shown with common centers in Fig. 7 and the values of the corresponding areas A_i are listed in Table I. The SdH frequencies observed by other workers[8] correspond very closely to those we observe for S_1 in the a direction, S_3 in the b direction, and $(S_1+S_2)/2$ in the c direction.

The orthorhombic symmetry of the crystal lattice does not allow us to identify unambiguously the location of the three pieces of Fermi surface from the SdH effect alone. However, since the band-structure calculation of Whangbo *et al.*[11] suggest that the Fermi surface is located at the Γ point in the Brillouin zone, we have assumed that all three observed surfaces have a common center at the center of the Brillouin zone. If this is the case, the observed surfaces S_1, S_2, and S_3 are mutually nested (i.e., a smaller surface always lying within the larger surface) with S_1 and S_2 nearly touching in the c direction while S_2 and S_3 are nearly touching the a direction. A three-dimensional representation of the nested Fermi surfaces is shown in Fig. 8. The radii r_i in the direction of the principal axes for each of the three surfaces S_1, S_2, and S_3 and their corresponding volumes are listed in Table I.

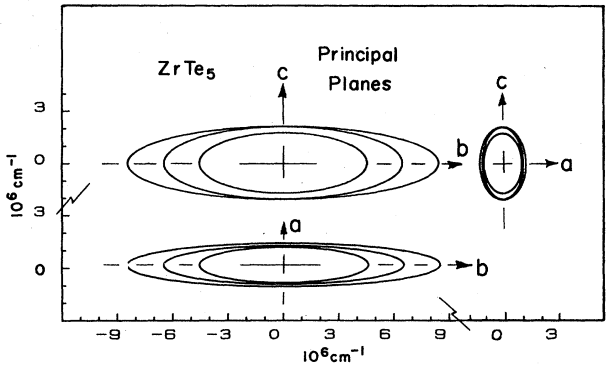

FIG. 7. Cross sections of the Fermi-surface ellipsoids in the three principal planes.

It is significant to note that to within our experimental accuracy, the volume of S_1 equals the sum of the volumes of S_2 and S_3. Since $ZrTe_5$ has an even number of electrons in the unit cell, it must be a compensated material. This suggests that the three ellipsoids observed do indeed

TABLE I. Fermi-surface dimensions and transport parameters of $ZrTe_5$.

	Units	Surface 1 holes	Surface 2 electrons	Surface 3 electrons
A_a	10^{12} cm^{-2}	55.8	42.5	24.2
A_b		8.4	7.2	5.7
A_c		32.8	22.4	14.5
r_a	10^6 cm^{-1}	1.26	1.10	1.05
r_b		8.35	6.51	4.41
r_c		2.13	2.08	1.74
V	10^{18} cm^{-3}	93.5	62.1	33.7
M_a	m_e	0.407	0.270	0.219
M_b		0.061	0.049	0.052
M_c		0.240	0.155	0.132
m_a	m_e	0.036	0.028	0.031
m_b		1.595	0.845	0.554
m_c		0.104	0.086	0.086
χ_a	K	4.47	1.90	1.90
χ_b		11.5	4.73	4.73
χ_c		4.78	1.83	1.83
T_a	10^{-13} s	2.7	6.4	6.4
T_b		1.1	2.6	2.6
T_c		2.5	6.7	6.7
τ_a	10^{-13} s	0.7	3.1	3.1
τ_b		3.7	9.5	9.5
τ_c		1.4	2.0	2.0

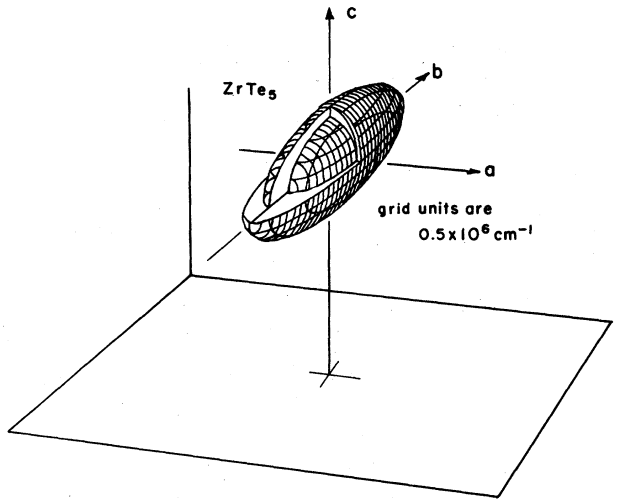

FIG. 8. A three-dimensional representation of the nested ellipsoidal Fermi surfaces.

constitute the entire Fermi surface and that surface S_1 is of one carrier type while surfaces S_2 and S_3 are of the opposite carrier type. Since the Hall effect and thermoelectric power measurements[12] show the dominant carrier at low temperatures to be electrons and since our effective mass and scattering rate measurements show S_2 and S_3 carriers to be more mobile than S_1 carriers (see below), one can reasonably identify the carriers of S_1 as holes and those of S_2 and S_3 as electrons. The measured hole surface S_1 has a volume about 2.5 times smaller and a somewhat lower anistropy than that predicted by the band calculation of Whangbo *et al.*[11] The combined electron surfaces and the hole surface each enclose approximately 3.0×10^{-4} of the zone volume and thus each constitutes only about 6.0×10^{-4} of an electron per unit cell.

The frequently seen combinations of frequencies, $(F_2+F_3)/2$ and (F_2+F_3), and the lack of similar combinations of F_1 with either F_2 or F_3 in any plane, can be explained in terms of magnetic breakdown orbits. Magnetic breakdown is possible between two orbits when, for a momentum value K, the Landau-level energy $(\hbar eH/M)$ exceeds the energy difference between the bands for a given k. Orbits then become possible which combine paths on two surfaces. If magnetic breakdown were to occur between hole and electron orbits it would yield crescent-shaped orbits having areas with corresponding difference frequencies $(F_1-F_2)/2$ rather than sums. Orbits of this shape have a lower probability of occurrence and indeed such difference frequencies were never observed. It should be pointed out, however, that at the predicted difference frequencies they would have been difficult to distinguish from artifacts arising from our background subtraction process. The magnetic breakdown that we find shows that surfaces S_2 and S_3 have a common center and are of the same carrier type, while S_1 is of opposite carrier type but not necessarily concentric with S_2 and S_3.

The band calculation of Whangbo *et al.*[11] gives Fermi surfaces substantially larger but similar in anisotropy to those which we observe experimentally; however, Whangbo's surfaces consist of one each of electron and hole portions of equal volume, both centered at Γ. Since their shapes differ, the two calculated surfaces must intersect. In contrast our three measured surfaces do not. The origin of a second electron surface of the shape we find is not easily explained within the framework of the calculation of Whangbo *et al.* Bullett's[5] band-structure calculations are, moreover, not well enough defined for a detailed comparison with experiment.

V. EFFECTIVE MASSES, DINGLE TEMPERATURES, AND SCATTERING TIMES

From the temperature and field dependences of the amplitude of the SdH oscillations, we have determined both the effective masses and Dingle temperatures that are associated with Fermi-surface orbits in the principal planes. The cyclotron effective mass is given implicitly by Eq. (1). In principle this mass can be obtained by measuring the temperature variation of the amplitude of a SdH oscillation at a given field. However, in practice, because of the presence of several frequencies, a moderately wide field range is needed to separate the peaks in the spectrum for the various orbits. Thus, it is also necessary to determine the appropriate "effective" field to associate with the spectrum amplitude measurement. To a good approximation[13] this field is given by the reciprocals of the mean of the reciprocals of the upper- and lower-field limits, i.e., the geometric mean. The amplitude-determination portion of this procedure, though accurate for independent oscillation components, may be less valid in the presence of magnetic breakdown. This is because the onset of magnetic breakdown orbits is at the expense of fundamental orbits. In the present case, since amplitudes of the oscillations from magnetic breakdown orbits are appreciably lower than those from the fundamentals, the errors can be expected to be relatively small.

Average cyclotron effective masses were measured in each of the principal directions and for each of the three surfaces, but the presence of noise seriously limited the accuracy of measurements for many field directions. The most accurate effective-mass determination was made with the field in the b direction. Consequently, it was decided that the best values for the effective masses are obtained as follows. Because of the small sizes and ellipsoidal shapes of the three pieces of Fermi surface, we assume a parabolic form for the electron and hole dispersion relationships, i.e.,

$$E(R)=\sum_{i=1}^{3}\frac{\hbar^2k_i^2}{2m_i}\ ,$$

where m_i is the effective mass in the ith direction. The above equation along with the definition of the cyclotron effective mass,

$$M_i=\frac{\hbar^2}{2\pi}\frac{\partial A_i}{\partial E}\ ,$$

where A_i is the cross-sectional area perpendicular to the field H_i, yield the following relations for M_a and M_c in terms of M_b and the areas (or frequencies):

$$M_a=(F_a/F_b)M_b \text{ and } M_c=(F_c/F_b)M_b \ , \tag{3}$$

where M_a, M_b, and M_c are the cyclotron effective masses for H parallel to the a, b, and c directions, respectively, and F_a, F_b, and F_c are the corresponding SdH frequencies. Similarly, the effective masses in the principal directions are given by

$$m_a=(F_c/F_a)M_b \ , \quad m_b=(F_aF_c/F_b^2)M_b \ , \quad m_c=(F_a/F_c)M_b \ . \tag{4}$$

The calculated cyclotron effective masses that were obtained were consistent with the measured values but, we believe, were more accurate. The SdH frequencies, the cyclotron effective masses, and the effective masses in the three principal directions are given in Table I.

The Dingle temperatures χ_i can be calculated from the SdH amplitude dependence on field once the effective masses are known [see Eq. (1)]. The Dingle temperature is that equivalent temperature increment which yields the same field dependence of the oscillations as does the impurity scattering. Although accurate values for the Dingle temperature for each orbit are hardly possible from the present data, rough values were obtained by measuring the field dependence of the amplitude separately at high fields where hole orbits predominate and at low fields where electron orbits predominate. Thus, we were able to obtain only a single scattering time for both electron surfaces. How accurately this reflects the actual situation, we cannot say. The cyclotron scattering time T_i is related to the Dingle temperature by the relation

$$T_i=\hbar/(2\pi k\chi_i)=1.2156\times10^{-12}/\chi_i \text{ sec} \ . \tag{5}$$

The values obtained for χ_i and for scattering times are summarized in Table I. The scattering times τ_i in the three principal directions can be found by assuming that τ has elliptical symmetry and then finding the τ which, when time averaged over the appropriate orbits, yields the experimentally determined T_i's. These results are shown in Table I. The accuracy of the individual SdH frequencies is $\pm2\%$, and of M_b, ±0.005. The accuracy of the derived quantities follows from these.

Assuming parabolic bands and using effective masses and dimensions in the principal axis directions, one can illustrate the band structure. This has been done for the directions Γ—a, Γ—b, and Γ—c and is given in Fig. 9, where the bands are drawn in the vicinity of the Fermi energy E_F. The value of k_BT at the resistivity peak (170 K) is indicated to illustrate that these bands are shallow and are substantially excited at temperatures of the resistivity peak and above.

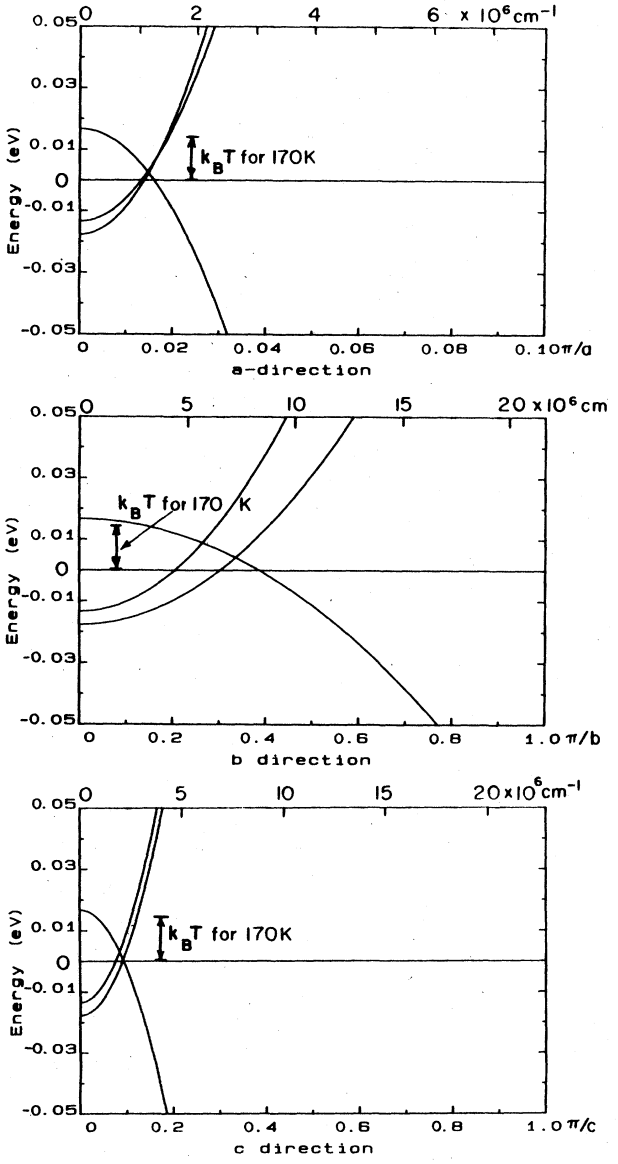

FIG. 9. The energy bands of $ZrTe_5$ in the three principal directions as suggested by the SdH data assuming parabolic bands. Distances from the zone center Γ are expressed both in reciprocal centimeters and as a fraction of the distance to a zone face. The value of k_BT at the resistance anomaly is indicated.

VI. DISCUSSION OF THE ANOMALOUS TRANSPORT PROPERTIES

It is of some interest to consider how these Fermiology results relate to current discussions regarding the possible existence of a CDW in $ZrTe_5$. On the basis of the low-temperature electronic structure alone, it is not possible to make any definitive statements. The small (semimetal-like) pieces of Fermi surface that we find at low temperatures could be representative of the electronic structure at temperatures well above all anomalous behavior, or they could be a consequence of a CDW-induced Brillouin-zone boundary. The electronic structure information that we have gathered, however, does delimit the possibilities as we now briefly discuss.

Since $ZrTe_5$ has an even number of electrons per unit crystallographic cell it must be a compensated metal in the absence of other sample periodicities, for example, a CDW. Thus, above the peak in the electrical resistivity there must be two or more sheets of Fermi surface with the total number of electrons equal to the total number of

holes. The introduction of a CDW that allows the retaining of a (new) low-temperature compensation, which is what we in fact find requires that (i) both the electron and hole surfaces be modified by the CDW, and (ii) the zone boundary associated with the CDW be additionally restricted in regard to its position in the Brillouin zone. Thus, the imposition of a CDW on a compensated system which gives rise to a new compensated system requires a much more specialized and therefore a much less probable set of physical circumstances than in systems which remain or become uncompensated.

On the other hand, if the electronic structure we have found is the same at room temperature, then our experimental results must serve substantially to influence the interpretations of the transport properties. The three surfaces we observe as having similar sizes and shapes also have mobilities that are not very different, and each has an E_F less than $k_B T$ above about 200 K. This structure is rather unusual and might be expected to give rise to unusual transport properties. Furthermore, the calculations of Whangbo *et al.*[11] show that the carriers' wave functions do not overlap very much, having consequences for the scattering. We have discussed some implications of these features elsewhere[14] and our work is continuing.

ACKNOWLEDGMENT

The authors would very much like to express their gratitude to Dr. Dale Peebles for many interesting and useful comments and suggestions.

[1]E. F. Skelton, T. J. Wieting, S. A. Wolf, W. W. Fuller, D. U. Gubser, T. L. Francavilla, and F. Levy, Solid State Commun, **42**, 1 (1982).

[2]C. M. Jackson, A. Zettl, G. Gruner, and F. J. DiSalvo, Solid State Commun. **45**, 247 (1983).

[3]F. J. DiSalvo, R. M. Fleming, and J. V. Wazczak, Phys. Rev. B **24**, 2935 (1981).

[4]S. Okada, T. Sambongi, M. Ido, Y. Tazuke, R. Aoki, and O. Fujita, J. Phys. Soc. Jpn. **51**, 460 (1982).

[5]D. W. Bullett, Solid State Commun. **42**, 691 (1982).

[6]A temperature-dependent anomaly in the intensity of "forbidden" x-ray lines which had been conceived of as possible evidence for a CDW (Ref. 1) has been shown to be probably an artifact from multiple reflections in imperfect crystals. S. B. Qadri and E. F. Skelton, private communication.

[7]S. Furuseth, L. Brattas, and A. Kjeklshus, Acta Chem. Scand. **27**, 8 (1973).

[8]M. Izumi, K. Uchinokura, R. Yoshizaki, S. Harada, T. Nakayama, A. Yamada, and E. Matsuura, J. Phys. (Paris) Colloq. **44**, C3-1705 (1983).

[9]A. Yamada, T. Nakayama, M. Izumi, R. Yoshizaki, K. Uchinokura, and E. Matsuura, in *Proceedings of the International Symposium on Nonlinear, Transport, and Related Phenomena in Quasi-One Dimensional Inorganic Conductors, Sapporo, Japan, 1983* (Hokkaido University Press, Sapporo, 1983), pp. 274–290.

[10]F. Levy and H. Berger, J. Cryst. Growth **61**, 61 (1983).

[11]M. H. Whangbo, F. J. DiSalvo, and R. M. Fleming, Phys. Rev. B **26**, 687 (1982).

[12]T. E. Jones, W. W. Fuller, T. J. Wieting, and F. Levy, Solid State Commun. **42**, 793 (1982).

[13]G. N. Kamm, J. Appl. Phys. **49**, 5951 (1978).

[14]A. C. Ehrlich, G. N. Kamm., D. J. Gillespie, and T. J. Wieting, Proceedings of the International Conference on the Physics and Chemistry of Low-Dimensional Synthetic Metals and International C.N.R. Symposium, Abano Terme, Italy 1984 [Mol. Cryst. Liq. Cryst. (to be published)].